Original article

Nuclear Medicine Communications

Feasibility assessment of yttrium-90 liver radioembolization imaging using amplitude-based gated PET/CT

Dustin R. Osborne, Shelley N. Acuff, Melissa L. Neveu, Mumtaz Syed, Austin D. Kaman and Yitong Fu

Purpose **The usage of PET/computed tomography (CT) to monitor hepatocellular carcinoma patients following yttrium-90 (^{90}Y) radioembolization has increased. Respiratory motion causes liver movement, which can be corrected using gating techniques at the expense of added noise. This work examines the use of amplitude-based gating on ^{90}Y-PET/CT and its potential impact on diagnostic integrity.**

Patients and methods **Patients were imaged using PET/CT following ^{90}Y radioembolization. A respiratory band was used to collect respiratory cycle data. Patient data were processed as both standard and motion-corrected images. Regions of interest were drawn and compared using three methods. Activity concentrations were calculated and converted into dose estimates using previously determined and published scaling factors. Diagnostic assessments were performed using a binary scale created from published ^{90}Y-PET/CT image interpretation guidelines.**

Results **Estimates of radiation dose were increased ($P < 0.05$) when using amplitude-gating methods with ^{90}Y PET/CT imaging. Motion-corrected images show increased noise, but the diagnostic determination of success, using the Kao criteria, did not change between static and motion-corrected data.**

Conclusion **Amplitude-gated PET/CT following ^{90}Y radioembolization is feasible and may improve ^{90}Y dose estimates while maintaining diagnostic assessment integrity.** *Nucl Med Commun* **39:222–227**

Nuclear Medicine Communications 2018, **39**:222–227

Keywords: gating, motion correction, PET/CT, radioembolization, yttrium-90 dosimetry, yttrium

Department of Radiology, University of Tennessee Graduate School of Medicine, University of Tennessee Medical Center, Knoxville, Tennessee, USA

Correspondence to Dustin R. Osborne, PhD, DABSNM, Molecular Imaging and Translational Research Program, University of Tennessee Medical Center, 1924 Alcoa Hwy, Knoxville, TN 37920, USA
Tel: +1 865 305 8264; fax: +1 865 305 8694; e-mail: dosborne@utmck.edu

Received 28 June 2017 **Revised** 6 December 2017
Accepted 7 December 2017

Introduction

Liver cancer is estimated to cause over 23 000 deaths per year in the USA and is expected to grow by 2.9–6.5% in the next 15 years [1]. Radioembolization using yttrium-90 (^{90}Y) spheres is a globally expanding palliative treatment option for patients with hepatocellular carcinoma [2]. SPECT imaging is typically used for assessment [3]; however, current systems lack robust quantitative capabilities, inhibiting their ability to produce accurate dosimetry calculations [4]. ^{90}Y-PET/computed tomography (CT) imaging following radioembolization has gained momentum as a method for dose assessment because of its ability to provide accurate quantitative dosimetry [5–7], despite low count rates from the low frequency of internal pair production [8] and image degradation caused by normal breathing patterns [9]. PET/CT dosimetry estimates can be used to quantitatively assess whether a given therapy delivery was successful or not [10].

Traditional phased-based gating can correct for motion, but results in noisier images with counts divided across each gate. Amplitude-based gating, available commercially as HD-Chest (Siemens Medical Solutions USA Inc., Knoxville, Tennessee, USA), is a software package that enables the ability to select a percentage of the amplitude of the respiratory cycle measured by a respiratory band that determines the data used in the final reconstruction [11]. Data reconstructed using amplitude gating methods have reduced motion compared with static acquisitions (Fig. 1), but with 2–5-fold less count loss compared with traditional phase-based gating [12]. This method has been shown to be effective in reducing motion artifacts and improving quantitative accuracy in routine clinical PET imaging [13]. In this technical note, we show the initial results that suggest that this technique may improve quantitative measurements without sacrificing potential diagnostic integrity because of increased image noise.

Patients and methods

Patient population

Informed consent was obtained from ten patients and the study was carried out under the auspices of a University of Tennessee Graduate School of Medicine Institutional Review Board-approved study (#3502). Patients ranged in age from 60 to 80 years and all underwent ^{90}Y radioembolization for the treatment of primary or metastatic hepatocellular carcinoma, followed by ^{90}Y PET/CT imaging. All patients in the study received SirSpheres

DOI: 10.1097/MNM.0000000000000794

Fig. 1

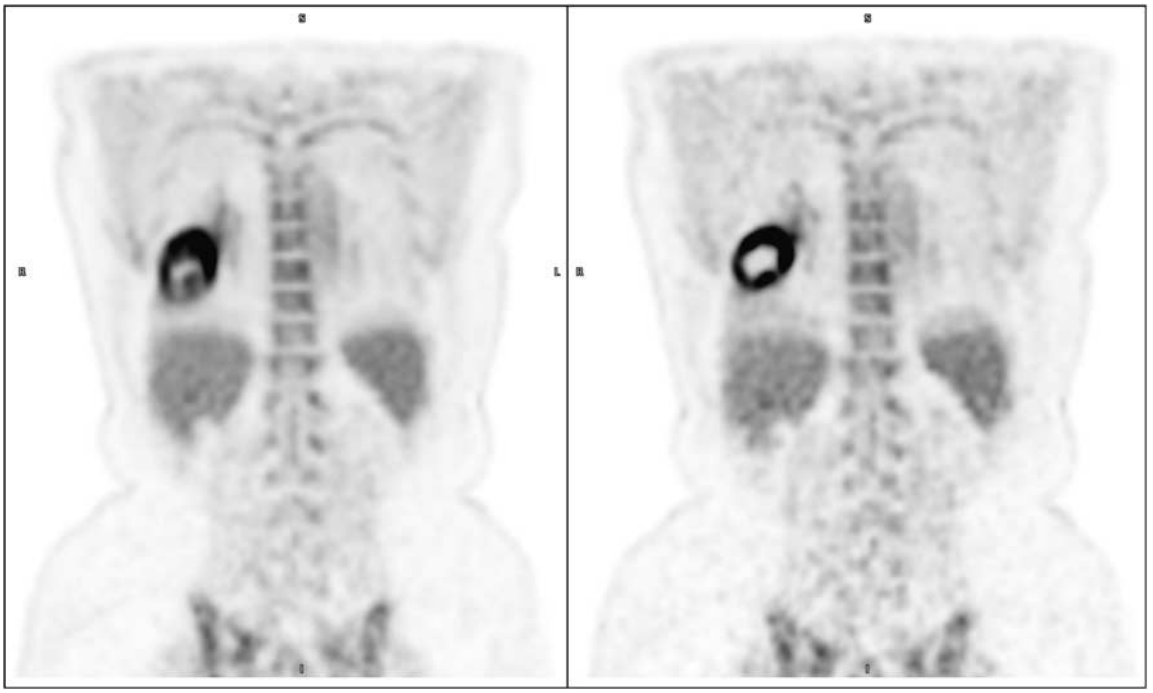

Motion-corrected (amplitude-based gating) (right) versus noncorrected (left) static image data. Images with motion artifacts can show severe distortions of the actual anatomy and can reduce quantitative accuracy. In this figure, we can observe a lesion in the left lobe that has a large necrotic center that is obscured considerably in the noncorrected image, but the detailed structure is more apparent in the motion-corrected image.

radioembolization therapy (SIRTeX Medical Limited, North Sydney, Australia) with standard of care lung shunt determinations [14] used to assess that they clinically qualify for radioembolization therapy.

Dose calculations

Dose-deposition estimates were calculated manually using the local deposition model. This model can be used to scale the activity concentration values measured using PET imaging to estimates of ^{90}Y dose deposition using the following equation:

$$D_{90_Y}\,(\mathrm{Gy}) = A_0\left(\frac{\mathrm{Bq}}{\mathrm{ml}}\right)\times K_{90_Y}\left(\mathrm{Gy}\times\frac{\mathrm{ml}}{\mathrm{Bq}}\right),$$

where the conversion factor K for ^{90}Y has been found previously in other research to be 4.782×10^{-5} Gy ml/Bq [7]. Using these methods, an estimate was obtained for the ^{90}Y dose deposited for each patient following their ^{90}Y radioembolization procedure.

Imaging protocol

All patients were imaged on a 64-slice, 4-ring Biograph mCT Flow (Siemens Medical Solutions USA Inc.). A 20–45 min listmode acquisition over the liver was performed for each patient using continuous bed motion acquisition. An Anzai respiratory band (Anzai Medical, Tokyo, Japan) was fitted around each patient to measure the respiratory cycle. The band was placed $\sim$5 cm from the top of the navel for each patient.

PET data were histogrammed into static (standard) and amplitude-based gated (corrected) datasets. Corrected data were reprocessed using the scanner default 30–35% amplitude threshold for reconstruction. All PET data were decay, branching ratio, attenuation, and scatter corrected using the standard systems and software provided on the Biograph mCT platform. No additional manual corrections were applied that could potentially introduce other biases not associated with the standard scanner hardware and software. Data were reconstructed using resolution recovery algorithms and time-of-flight corrections (200×200 image matrix, 1 iteration, 21 subsets, 2 mm Gaussian filter per previous assessments performed on this system [7]). Nongated CT data were acquired for anatomical segmentation at 120 kVp using a continuously modulated tube current and 5 mm slices (512×512 image matrix, 1 mm^3 Gaussian filter).

Data analysis

Three methods were used to assess the impact of amplitude gating on delivered ^{90}Y dose deposition estimates compared with static imaging. Two of the assessments use PET data voxel value thresholding to draw region of interests (ROIs) using CT segmented liver regions as threshold boundaries. The third assessment

used CT data to segment individual primary lesions and use those ROIs transferred to the PET image voxels to assess ^{90}Y dose deposition. All regions of interest were drawn using the Inveon Research Workplace (Siemens Healthineers, Knoxville, Tennessee, USA).

Two threshold settings were used for image analysis as represented in Fig. 2. The first method used a standard style image threshold that is used in commonly nuclear medicine analysis with a lower bound determined by 30% of the maximum value in the lesion (henceforth referred to as the 30 maximum threshold method). The second method (region-based threshold method) used a lower bound derived from the maximum of several ROIs drawn in the healthy parenchyma of the embolized liver, with the upper bound of both thresholds set to the maximum pixel value in the reconstructed PET image. This method enables improved comparison of static and gated data as increases in high-frequency noise will also propagate into the regions used to set the lower threshold limit. The third method (individual lesion method) involved segmentation of 17 individual primary lesions across all patients using the fused PET/CT data and voxel values from the PET images used for conversion to ^{90}Y dose deposition estimates. For each ROI, the mean, minimum, maximum, and SD of the activity concentration were recorded as well as the ROI volume. ROI activity concentration values were then multiplied by the above-mentioned conversion factor of 4.78×10^{-5} to convert from activity concentration (Bq/ml) into an absorbed dose estimate (Gy) [15]. Measured values were compared statistically between static and amplitude-gated scan types as well as the final recorded estimates of the ^{90}Y dose obtain from the final therapy radiology reports.

Fig. 2

Example regions of interest using the threshold techniques described in the Materials and methods section. The two different threshold methods provide slightly different region of interest sizes. The 30 maximum threshold is represented by the light gray outline, whereas the region-based threshold method is represented by a single black line outline.

Diagnostic assessment

Data were assessed clinically by a board-certified nuclear medicine physician using the methods described by Kao *et al.* [10], which are diagnostic criteria developed to assess the quality of the ^{90}Y therapy delivery as opposed to the diagnosis of the patient's disease. A binary scoring system based on Kao *et al.*'s [10] methods, shown in Table 1, was created with the inclusion of an additional parameter to compare activity 'bleeding' on standard and corrected datasets. A score of 1 indicated that the given criteria were fulfilled, whereas a score of 0 indicates that the criteria were not fulfilled. Cumulative scores were compared between methods to assess any changes in diagnostic image interpretation. A window/level threshold of 25% of maximal intensity was used for all patients for the visual diagnostic assessment.

Results

Quantitative assessment

ROI volumes were found to be significantly reduced for all threshold methods when using motion-corrected data versus the standard images. Volumes of ROIs drawn on motion-corrected images were reduced by an average of 36 and 79% percent for 30 maximum and region-based threshold methods, respectively, in the global liver analyses. Individual lesion analysis yielded average volume reductions of 16%. The maximum reductions observed for global and local lesion analysis were greater than 40 and 60%, respectively. Statistics collected for volume changes are shown in Table 2.

Mean dose calculations in global liver analyses were shown to be underestimated by an average of 23% using region-based thresholding (Table 3). Individual lesion analysis indicated an average underestimation of dose of 8%. Higher standard deviations were observed in corrected images, with the average increase for region-based threshold methods being 12% for global liver calculations and 15% for individual lesion assessments. Calculations of coefficient of variation indicated a reduction of 19 and 28%, respectively.

With one exception, all measurements of maximum values comparing standard images with those using amplitude-based gating were statistically significant with P value less than 0.05. Post-hoc power analysis indicated

Table 1 Binary rating scale on the basis of the Kao criteria

^{90}Y Binary criteria
Technical success criteria fulfilled – 0/1
Unsuccessful criteria not fulfilled – 0/1
Nontarget activity criteria not fulfilled – 0/1
Noise spike criteria not fulfilled – 0/1
Uncorrected motion 'bleeding' – 0/1

The Kao criteria are a clinical assessment of diagnostic data acquired from postradioembolization PET/CT. For this work, we developed a binary scale on the basis of these criteria to enable a quantitative assessment of the diagnostic quality of the therapy delivery.
CT, computed tomography; ^{90}Y, yttrium-90.

that we attained more than 90% and more than 80% power for global and local assessments, respectively, even with the small number of patients used in this initial assessment. Values of estimated maximum dose are presented in Table 4. All percent changes in values are presented in Table 5.

The mean and standard deviation of estimated delivered doses recorded in the radiology reports for all 10 patients following radioembolization was 130.74 ± 56 Gy. The 30 maximum threshold method resulted in underestimation of the actual dose for both static and amplitude-gated datasets with underestimations of 37 and 34%, respectively. For the region-based thresholding method, static data underestimated dose by 20% whereas amplitude-gated data underestimated dose by only 5%. These percentages can be derived from the mean calculated dose values found in Table 3.

Diagnostic assessment

Diagnostic assessments of data indicated an observed increase in image noise for motion-corrected data, with noise spike criteria fulfilled in 100% of all motion-corrected cases compared with 18% for standard static imaging. Criteria for technical success, according to the Kao criteria, were fulfilled in all patients analyzed, with no patients showing signs of unsuccessful treatment or off-target activity. Bleeding of activity into areas around treatment regions in nonmotion-corrected PET images was observed in 82% of cases. Figure 3 shows a comparison image that shows the reduced blur in motion-corrected images at the expense of additional noise.

Table 2 Descriptive statistics calculated for volume measurements derived from each of the three segmentation methods described in this work

	Static imaging		Amplitude gating	
Volume (mm^3)	Mean ± SD ($\times 10^6$)	Minimum/maximum ($\times 10^6$)	Mean ± SD ($\times 10^6$)	Minimum/maximum ($\times 10^6$)
30 Maximum	2.35 ± 5.19	2.29/17.10	1.50 ± 2.63	0.21/89.40
Region-based	0.624 ± 0.19	0.20/0.84	0.47 ± 0.17	0.16/0.76
Individual Lesion	0.12 ± 0.08	0.01/0.25	0.11 ± 0.08	0.008/0.23

Mean, SD, minimum, and maximum values are presented for each segmentation method drawn on both static and motion-corrected (amplitude gated) images.

Discussion

Quantitative metrics show that the amplitude gating methods described here generally increased values for dose estimates from PET/CT imaging, which may be underestimated because of respiratory motion. Although image noise increases as a result of count loss when using gating methods, the coefficient of variation decreased by an average of 19%. This suggests that improved event localization led to higher mean values that helped compensate for increased noise. ROI volumes also showed statistically significant reductions for threshold-based methods, which is most likely the result of the combined effects of both decreased motion blur making apparent tumor volumes smaller and the impact of increased high-frequency noise in the data from reduced counts.

Diagnostic scoring of images showed that the increase in image noise in corrected images did not result in a change in the determination of whether a procedure was successful or unsuccessful. Also, increased noise did not have any effect on the assessment of off-target activity, which could be a concern with radioembolization procedures [16].

Statistical significance was observed when comparing standard and motion-corrected values, with an estimated post-hoc power of 0.9 and 0.8 for global and individual lesion measurements, respectively. One measurement in the global analysis was observed to be nonsignificant, but was determined to likely be the result of a type II statistical error.

Standard imaging showed an average underestimation of maximum dose of 40%, which may be significant if using ^{90}Y PET/CT to verify ^{90}Y dose. This work shows initial results that suggest that the use of amplitude-based respiratory motion correction may be a useful tool for post ^{90}Y-radioembolization PET/CT.

Conclusion

The use of amplitude-based gated PET/CT imaging in post-^{90}Y radioembolization assessment is clinically feasible. We have shown initial results that amplitude-based gating can be used to improve dose estimates with minimal impact on diagnostic assessment of therapy delivery using the Kao criteria. Further clinical studies are required to fully test the results of this initial feasibility study; however, the ease of such a method for

Table 3 Descriptive statistics calculated for measurements of the mean dose derived from each of the three segmentation methods described in this work

	Static imaging		Amplitude gating	
Mean dose (Gy)	Mean ± SD	Minimum/maximum	Mean ± SD	Minimum/maximum
30 Maximum	82.1 ± 80.5	5.4/289.6	86.8 ± 86.9	8.7/313.5
Region-based	105.0 ± 88.4	43.5/342.0	125.0 ± 102.0	52.6/404.0
Individual lesion	149.8 ± 101.3	51.4/408.0	156.2 ± 107.1	49.9/430.0

Mean, SD, minimum, and maximum values are presented for each segmentation method drawn on both static and motion-corrected (amplitude gated) images.

Table 4 Descriptive statistics calculated for measurements of maximum dose derived from each of the three segmentation methods described in this work

	Static imaging		Amplitude gating	
Maximum dose (Gy)	Mean ± SD	Minimum/maximum	Mean ± SD	Minimum/maximum
30 Maximum	319.32 ± 209.3	137.7/725.7	355.6 ± 239.8	158.3/835.2
Region-based	525.0 ± 332.0	198.0/1.080.0	658.0 ± 387.0	297.0/1.350.0
Individual lesion	286.8 ± 186.0	94.2/717.0	309.9 ± 207.4	88.8/828.0

Mean, SD, minimum, and maximum values are presented for each segmentation method drawn on both static and motion-corrected (amplitude gated) images.

Table 5 Region of interest percentage differences for varying threshold methods

Metric	Average change (30%)	Maximum change (30%)	Average change (region-based)	Maximum change (region-based)
Volume	36	48	79	41
Mean	6	62	23	37
Minimum	11	25	80	91
Maximum	11	25	40	82

Percentage differences for each thresholding method have been calculated.

Fig. 3

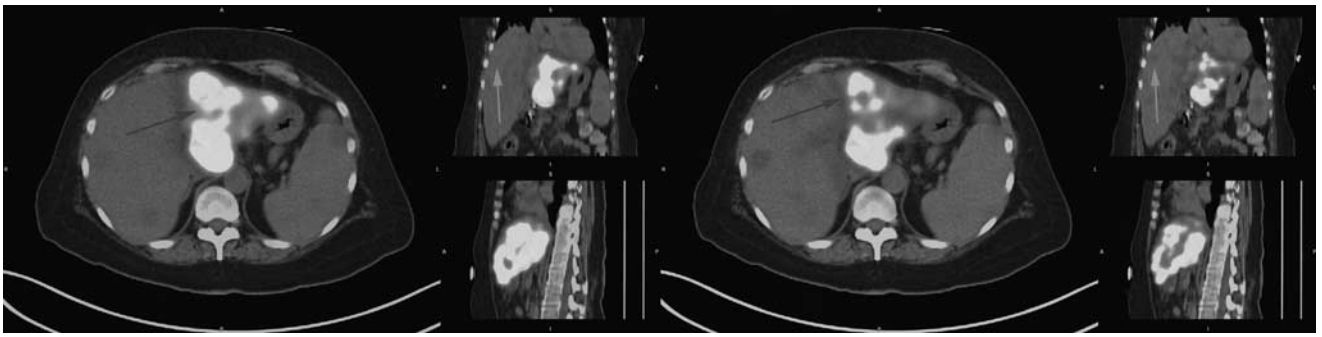

A comparison of amplitude-gated motion-corrected yttrium-90 PET/computed tomography (CT) with standard static PET/CT images. The corrected image displayed on the right, shows improved resolution (dark gray arrow) with increased noise spike artifacts (light gray arrow).

routine clinical use warrants publication of these initial findings.

Acknowledgements

The University of Tennessee maintains ongoing collaborations with Siemens Medical Solutions USA Inc.

Dustin Osborne and Shelley Acuff occasionally provide expert testimonial to Siemens Medical Solutions USA Inc.

Some results of this work have been presented at the Society of Nuclear Medicine and Molecular Imaging over the last 2 years.

Conflicts of interest

There are no conflicts of interest.

References

1 Rahib L, Smith BD, Aizenberg R, Rosenzweig AB, Fleshman JM, Matrisian LM. Projecting cancer incidence and deaths to 2030: the unexpected burden of thyroid, liver, and pancreas cancers in the United States. *Cancer Res* 2014; **74**:2913–2921.

2 Bilbao JI, Reiser MF. *Liver radioembolization with ^{90}Y microspheres*. Heidelberg: Springer; 2014.

3 Ahmadzadehfar H, Muckle M, Sabet A, Wilhelm K, Kuhl C, Biermann K, *et al*. The significance of bremsstrahlung SPECT/CT after yttrium-90 radioembolization treatment in the prediction of extrahepatic side effects. *Eur J Nucl Med Mol Imaging* 2012; **39**:309–315.

4 Ljungberg M, Frey E, Sjogreen K, Liu X, Dewaraja Y, Strand SE. 3D absorbed dose calculations based on SPECT: evaluation for 111-In/90-Y therapy using Monte Carlo simulations. *Cancer Biother Radiopharm* 2003; **18**:99–107.

5 Dieudonne A, Garin E, Laffont S, Rolland Y, Lebtahi R, Leguludec D, *et al*. Clinical feasibility of fast 3-dimensional dosimetry of the liver for treatment planning of hepatocellular carcinoma with ^{90}Y-microspheres. *J Nucl Med* 2011; **52**:1930–1937.

6 Ng SC, Lee VH, Law MW, Liu RK, Ma VW, Tso WK, *et al*. Patient dosimetry for ^{90}Y selective internal radiation treatment based on ^{90}Y PET imaging. *J Appl Clin Med Phys* 2013; **14**:212–221.

7 Pasciak AS, Bourgeois AC, Bradley YC. A comparison of techniques for (^{90})Y PET/CT image-based dosimetry following radioembolization with resin microspheres. *Front Oncol* 2014; **4**:121.

8 Greenberg JS, Deutsch M. Positrons from the decay of P32 and Y90. *Phys Rev* 1956; **102**:415–421.

9 Polycarpou I, Tsoumpas C, King AP, Marsden PK. Impact of respiratory motion correction and spatial resolution on lesion detection in PET: a simulation study based on real MR dynamic data. *Phys Med Biol* 2014; **59**:697–713.

10 Kao YH, Steinberg JD, Tay YS, Lim GK, Yan J, Townsend DW, *et al*. Post-radioembolization yttrium-90 PET/CT – part 1: diagnostic reporting. *EJNMMI Res* 2013; **3**:56.
11 Van Elmpt W, Hamill J, Jones J, De Ruysscher D, Lambin P, Ollers M. Optimal gating compared to 3D and 4D PET reconstruction for characterization of lung tumours. *Eur J Nucl Med Mol Imaging* 2011; **38**:843–855.
12 Pépin A, Daouk J, Bailly P, Hapdey S, Meyer ME. Management of respiratory motion in PET/computed tomography: the state of the art. *Nucl Med Commun* 2014; **35**:113–122.
13 Van Der Gucht A, Serrano B, Hugonnet F, Paulmier B, Garnier N, Faraggi M. Impact of a new respiratory amplitude-based gating technique in evaluation of upper abdominal PET lesions. *Eur J Radiol* 2014; **83**:509–515.
14 Radiology ACo. Rosenthal S, Yung E, Zaki B, Salem R, Coldwell D, Murthy R, *et al*. ACR–SIR practice parameter for radioembolization with microsphere brachytherapy device (RMBD) for treatment of liver malignancies. In: Rosenthal S, Yung E, Zaki B, Salem R, Coldwell D, Murthy R, *et al*, editors. *American College of Radiology Practice Guidelines*. Society of Interventional Radiology: Fairfax, Virginia; 2014. p. 23.
15 Bourgeois AC, Chang TT, Bradley YC, Acuff SN, Pasciak AS. Intraprocedural yttrium-90 positron emission tomography/CT for treatment optimization of yttrium-90 radioembolization. *J Vasc Interv Radiol* 2014; **25**:271–275.
16 Lewandowski RJ, Salem R. Yttrium-90 radioembolization of hepatocellular carcinoma and metastatic disease to the liver. *Semin Interv Radiol* 2006; **23**:64–72.